# High-pressure effect on inverse spinel $LiCuVO_4$: X-ray diffraction and Raman scattering*

Liang Heng-Nan(梁桁楠), Ma Chun-Li(马春丽), Du Fei(杜 菲), Cui Qi-Liang(崔啟良)†, and Zou Guang-Tian(邹广田)

*State Key Laboratory of Superhard Materials, College of Physics, Jilin University, Changchun* 130012, *China*

(Received 28 August 2012; revised manuscript received 12 October 2012)

The effect of external quasi-hydrostatic pressure on the inverse spinel structure of $LiCuVO_4$ was studied in this paper. High-pressure synchrotron X-ray diffraction and Raman spectroscopy measurements were carried out at room temperature up to 35.7 and 40.3 GPa, respectively. At a pressure of about 20 GPa, both Raman spectra and X-ray diffraction results indicate that $LiCuVO_4$ was transformed into a monoclinic phase, which remained stable up to at least 35.7 GPa. Upon release of pressure, the high-pressure phase returned to the initial phase. The pressure dependence of the volume of low pressure orthorhombic phase and high-pressure monoclinic phase were described by a second-order Birch–Murnaghan equation of state, which yielded bulk modulus values of $B_0 = 197(5)$ and 232(8) GPa, respectively. The results support the empirical suggestion that the oxide spinels have similar bulk modulus around 200 GPa.

**Keywords:** high pressure, inverse spinel $LiCuVO_4$, X-ray diffraction, Raman scattering

**PACS:** 61.50.Ks **DOI:** 10.1088/1674-1056/22/1/016103

## 1. Introduction

Spinel structural materials with the formula of $AB_2O_4$, as one kind of ternary oxides, have always been a focus since they have extensive and significant applications in many aspects. For example, these materials have been considered as battery materials, magnetic materials, superhard materials, and luminescent materials.[1–5] According to the distribution of atoms A and B on the lattice sites, the spinel structural materials can be classified into two distinct kinds, known as the normal and inverse spinels, respectively. The normal spinel is characterized by that the A and B atoms occupy the tetrahedral and octahedral sites, respectively, whereas in the inverse spinel structure, a part of B atoms occupy the tetrahedral sites, the A and the remaining B atoms occupy the octahedral sites.

Recently, one of the spinel structural multiferroic materials, namely, a cuprate with the chemical formula $LiCuVO_4$ was synthesized. $LiCuVO_4$ is in an orthorhombic distorted inverse spinel structure with the space group *Imma* ($D_{2h}^{28}$), with the lattice constants $a = 5.662$ Å, $b = 5.809$ Å, and $c = 8.758$ Å (see Fig. 1). The component atoms of $LiCuVO_4$ in a unit cell occupy the following positions: Cu(4*a*) at (0, 0, 0), Li(4*d*) at (1/4, 1/4, 3/4), V(4*e*) at (0,1/4, 0.386), $O_1$(8*h*) at (0, 0.0164, 0.2748), and $O_2$(8*i*) at (0.2352, 1/4, 0.9993). The detailed crystallographic data and a picture of the structure of $LiCuVO_4$ are given by Lafontaine *et al*.[6] Jahn–Teller distortions, however, usually happen in these structures. The orthorhombic distortion results from a cooperative Jahn–Teller effect of the $Cu^{2+}$ ions at the octahedral sites.[7] The nonmagnetic $V^{5+}$ ions occupy the tetrahedrally coordinated A sites, while $Li^+$ and $Cu^{2+}$ occupy the B positions within the oxygen octahedra of the spinel structure. Both $LiO_6$ and $CuO_6$ octahedra form independent chains along *a* and *b* directions, respectively, which themselves build a stack of independent planes of Li and Cu rods along the *c* direction.[8] The $CuO_6$ octahedra forms independent and infinite chains along the *b* direction, leading to two nearly rectangular Cu–O–Cu superexchange paths between nearest neighbor copper ions. Due to the peculiar distribution and valencies of the metal cations in this structure are of great importance for the interpretation of the magnetic, electric and crystallographic properties. $LiCuVO_4$ can be viewed as multiferroic material in which the magnetic and ferroelectric properties coexist. As a result, a promising application of $LiCuVO_4$ as both a magnetic material and a lithium cell material is expected.[9–13]

High pressure is an effective way to explore the structures and phase transitions of materials. A number of high pressure experiments have been performed on the spinel materials. However, most of them are about cubic or tetragonal spinels.[14–17] To our knowledge, no orthorhombic inverse spinel structure of ternary oxides have been studied under high pressure. In this paper, in-situ X-ray diffraction and Raman scattering measurement were carried out to explore the pressure-induced phase transition of polycrystalline $LiCuVO_4$. The results will help to elucidate the structure characteristics and dynamics of the pressure induced phase transformation relating to the structure of spinel family.

*Project supported by the National Natural Science Foundation of China (Grant Nos. 11074089 and 11004073) and the National Basic Research Program of China (Grant No. 2011CB808200).

†Corresponding author. E-mail: cql@jlu.edu.cn

© 2013 Chinese Physical Society and IOP Publishing Ltd 

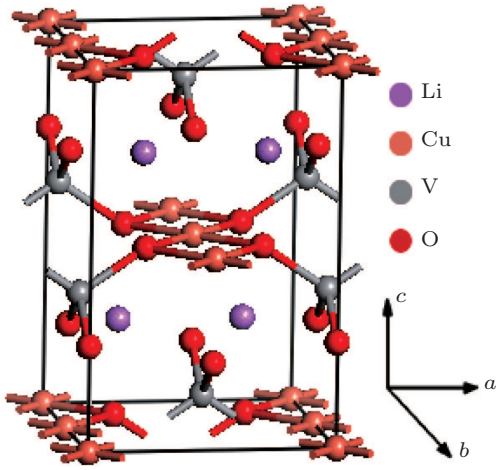



**Fig. 1.** (color online) The crystal structures of orthorhombic $LiCuVO_4$ with *Imma* space group at atmosphere. Li ions are in purple. Cu, V, and O ions are in pink, grey, and red, respectively.

## 2. Experiment

The polycrystalline sample $LiCuVO_4$ was prepared by solid-state reaction at 550 °C, with $Li_2CO_3$, $Cu_2O$, and $V_2O_5$ as the starting materials, which were weighed in a stoichiometric ratio. Detailed information of the synthesis was reported in Refs. [18] and [19]. High-pressure XRD and Raman measurements were conducted at room temperature by using a gasketed high-pressure Mao–Bell–type diamond anvil cell (DAC) with a diamond culet face of 400 μm in diameter. The synthesized sample and ruby particles were loaded into the high-pressure chamber. The chamber is a small hole (120 μm diameter and 50 μm thickness) which was drilled at the center of a T-301 stainless steel gasket and filled with a mixture of 16:3:1 of methanol/ethanol/water as the pressure-transmitting medium. The pressure was determined from the frequency shift of the ruby $R_1$ fluorescence line.[20] By monitoring the separation and the width of the ruby $R_1$ and $R_2$ peaks, it determined that our experiments were conducted under the quasi-hydrostatic condition. In situ high-pressure angle-dispersive XRD experiments were carried out up to 35.7 GPa at the B2 station of Cornell High Energy Synchrotron Source (CHESS), Wilson Laboratory, Cornell University.[21] A monochromatic beam with a wavelength of 0.4859 Å was used. The diffraction data were collected using an MAR345 detector. The two-dimensional XRD images were analyzed using FIT2D software, yielding one-dimensional intensity versus diffraction angle $2\theta$ patterns. The average acquisition time was 400 s. The sample–detector distance and geometric parameters were calibrated using a $CeO_2$ standard from the National Institute of Standards and Technology (Gaithersburg, MD). Simulation and analysis of the XRD patterns at different pressures were performed using the Material Studio program. During each refinement cycle, the scale factor, background parameter, and cell parameter were optimized. High-pressure Raman spectra were recorded on a Renishaw inVia Raman Microscope in the backscattering geometry using the 633 nm line of a He-Ne laser, provided with a charge coupled device (CCD) detector system. A 3-min exposure time was used at each Raman collected run in average.

## 3. Results and discussion

### 3.1. High-pressure Raman spectra

Raman spectroscopy provides valuable information on local and cooperative changes during pressure-induced transformations between each phase.[22] Thus, the in-situ Raman scattering of the polycrystalline compound $LiCuVO_4$ has been conducted under high pressure. According to group theory analysis, $LiCuVO_4$ has the following set of phonon modes:[23] 15 Raman-active modes, $5A_g+2B_{1g}+4B_{2g}+4B_{3g}$; 20 IR-active modes, $8B_{1u}+6B_{2u}+6B_{3u}$; 4 inactive modes, $4A_u$. In addition, detailed Raman studies of $LiCuVO_4$ have discussed the assignments of different mode frequencies. A compilation of the optical phonon frequencies, the symmetry and pressure dependences are given in Table 1.

**Table 1.** Observed Raman vibration modes of $LiCuVO_4$ at ambient conditions, their assignments, and pressure dependences.

| Assignment | Observed modes at 1 atm/$cm^{-1}$ | Raman shift/$cm^{-1}\cdot GPa^{-1}$ | | |
|---|---|---|---|---|
| | | < 20 GPa | 20–24.5 GPa | > 24.4 GPa |
| $A_g$ | 152 | 2.26 | – | – |
| $A_g$ | 186 | 1.49 | – | – |
| $B_{3g}$ | 213 | 2.41 | – | – |
| $B_{1g}$ | 230 | 1.57 | – | – |
| $B_{2g}$ | 248 | 1.69 | – | – |
| $A_g$ | 305 | 1.57 | 0.73 | 1.18 |
| $B_{1g}$ | 353 | 0.779 | 1.34 | 2.39 |
| $A_g$ | 450 | 2.73 | – | – |
| $B_{2g}$ | 588 | – | – | – |
| $A_g$ | 742 | 4.55 | 1.05 | 2.37 |
| $B_{3g}$ | 848 | 2.87 | – | – |
| $A_g$ | 873 | 2.30 | 2.34 | 0.64 |

Table 1 and Figure 2 shows that all Raman-active phonon modes are discernible at ambient conditions, at the same time all the observed modes correspond well to those reported in the literature.[23] However, these observed Raman modes can be classified into three general families of lattice vibrations. In the high-frequency range (650–1000 $cm^{-1}$), the vibration mode is the stretching of the distorted $VO_4$ groups. Therefore, fours peak of Raman spectrum ($2A_g+B_{2g}+B_{3g}$) in high-frequency range correspond to the stretching V–$O_1$ and V–$O_2$ vibration. In the intermediate-frequency (400–650 $cm^{-1}$) region the peaks are often related to complex vibrations, involving the simultaneous participation of all cations, tetrahedral and octahedral.[24] The bands with frequencies below 400 $cm^{-1}$ can be assigned to complex vibrations with a predominant contribution of the $Li^+$ and $Cu^{2+}$ cations. Figure 2 shows the representative Raman bands of $LiCuVO_4$ in the frequency range of 100–1100 $cm^{-1}$ at different pressures under hydrostatic compression.

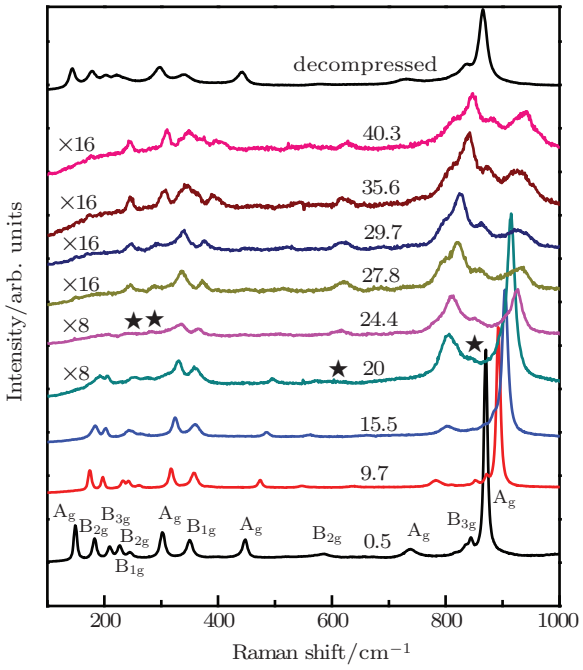



**Fig. 2.** (color online) The Raman spectra of $LiCuVO_4$ at various pressures up to 40.3 GPa.The assignment of the experimentally observed Raman peaks is based on the theoretical analysis of Shirokov *et al*. Pentagon symbols show the appearance of new Raman peaks. ×8 and ×16 mean increased 8 and 16 times of intensity, respectively. The top panel is a Raman spectrum at atmosphere after decompressing from 40.3 GPa.

According to Fig. 2 we can see that there is no shape change in the Raman pattern below 20 GPa, except that the three peaks at nearby 220 $cm^{-1}$, and the two peaks at high frequencies nearby 850 $cm^{-1}$ exhibit the variation in profile and in intensity, as shown in their merging, broadening and losing intensity before the phase transformation (Fig. 2 and Table 1). The rest of the Raman peak shifted toward high frequencies due to compression. However, starting from 20 GPa, the intensity of Raman signal diminished abruptly. We enlarge the XRD pattern intensity by 8 times so as to observe the details of Raman peak clearly. At the beginning of the 20 GPa Raman pattern, new Raman peaks appear at 246, 286, 613, and 854 $cm^{-1}$ as marked by asterisks. Furthermore, with increasing pressure, the lower-frequency Raman peaks below 300 $cm^{-1}$ complete extinction. In addition, the peak which belongs to $A_g$ vibration mode round 900 $cm^{-1}$ lose intensity quickly. By contrast, the intensity of the other peak which also belong to the $A_g$ vibration mode around 800 $cm^{-1}$ increases gradually with increasing pressure. These changes suggest that a phase transition occurred in the sample. The pressure dependence of Raman phonon frequencies also shown in Fig. 3. There were same apparent discontinuities onset at same pressure range on all modes. It further proved that a structural transformation occurred from 20 to 24 GPa. The phase transition requires XRD to identify.

Upon release of pressure, this high-pressure phase transformed back to the atmospheric $LiCuVO_4$ phase by the same way, and it stably returned to ambient conditions. The Raman spectrum at atmosphere after decompressing from 40.3 GPa is display at the top of Fig. 2. At ambient conditions, the obtained Raman spectrum of decompression is consistent to the spectrum that was collected from the unpressurized one before. Therefore, it indicated that the whole phase transition course is reversible.

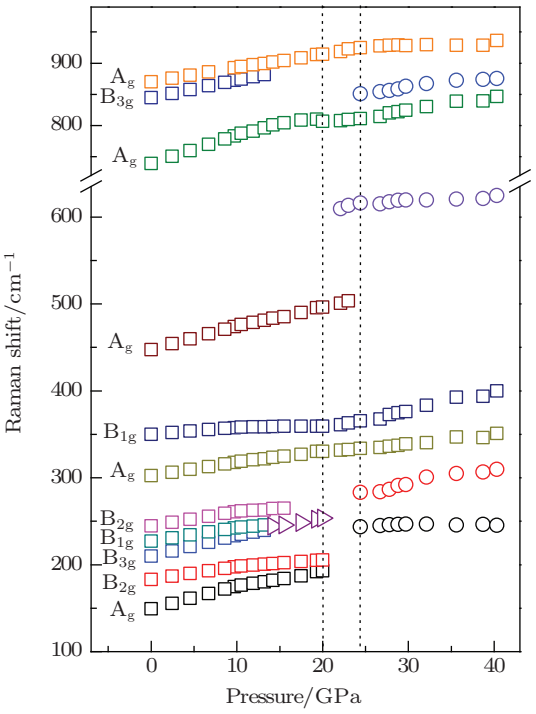



**Fig. 3.** (color online) Pressure dependence of Raman frequency shifts in $LiCuVO_4$ during compression from 0 to 40.3 GPa. The middle regions correspond to two phase coexistence. Different modes are labeled.

### 3.2. High-pressure synchrotron radiation X-ray diffraction

High-pressure synchrotron radiation X-ray diffraction provides significant structural information and the most powerful evidence for determining the transformations during pressure-induced transition between each phase.[25] Because of this, the in-situ high pressure XRD experiment of $LiCuVO_4$ in DAC was performed at various pressures up to 35.8 GPa. The XRD patterns of $LiCuVO_4$ were collected by increasing the pressure shown in Fig. 4. Rietveld refinements were carried out at the pressures below 21.7 GPa using MATERIALS STUDIO software to obtain the cell parameters. At ambient conditions, all the diffraction peaks are indexed to an orthorhombic structure with the space group of *Imma* and lattice constants of $a = 5.664(3)$ Å, $b = 5.795(6)$ Å, $c = 8.729(5)$ Å, and $V_0 = 285.53(2)$ Å$^3$. The number of molecules of this phase per unit cell ($Z$) is 4. The Rietveld refinement of XRD obtained at 1.5 GPa is shown in Fig. 6(a). It shows a good agreement with the orthorhombic structure. The $d$-spacing of $LiCuVO_4$ as a function of pressure (see Fig. 5) clearly shows that some of the peaks are initially shift limited, and hence, gradually display the regular pressure dependence. Upon a continuous enhancement of pressure, all of the diffraction lines shift toward higher angles accompanied by a change of relative intensities. As the pressure increases to 21.7 GPa, some new diffraction peaks (marked with asterisks) start to appear in the XRD patterns (see Fig. 4), indicating the onset of a structural phase transition. Two new peaks appear at $2\theta = 9.16(3)^\circ$ and $9.62(9)^\circ$ emerges beside the parent merged peak of (112) and (200) which belong to the orthorhombic phase, while another new peak appear at $2\theta = 13.70(2)^\circ$. The high pressure phase and the orthorhombic phase coexist up to about 21.7 GPa. There is a pressure range where the two phases coexist, which might be explained as being due to the large kinetic effects of the first-order transition. Following the pressure reach to 24.5 GPa, all of the six new diffraction peaks emerge, otherwise some diffraction parent peak of the orthorhombic phase are undetectable, which indicated that the sample is fully converted to the new high phase. When the pressure further increases to 35.7 GPa, there are no shape change peaks observed. Thus, it is believed that the new high-pressure phase remains to 35.7 GPa. Upon release of pressure, the high-pressure phase transforms back to the ambient phase, indicating that orthorhombic–monoclinic phase transition is fully reversible. It is consistent with the results of Raman measurement.

The change of $d$-spacing as a function of pressure at room temperature is shown in Fig. 5. The discontinuity shifts of the $d$-spacing onset at 20–24 GPa provide a further evidence of phase transition. According to the XRD pattern of the new phase under high-pressure, we perform the refinement work to discuss the new phase information. Pawley refinement is used for the X-ray diffraction peaks at the pressures of which above 24.5 GPa to obtain the structural data.

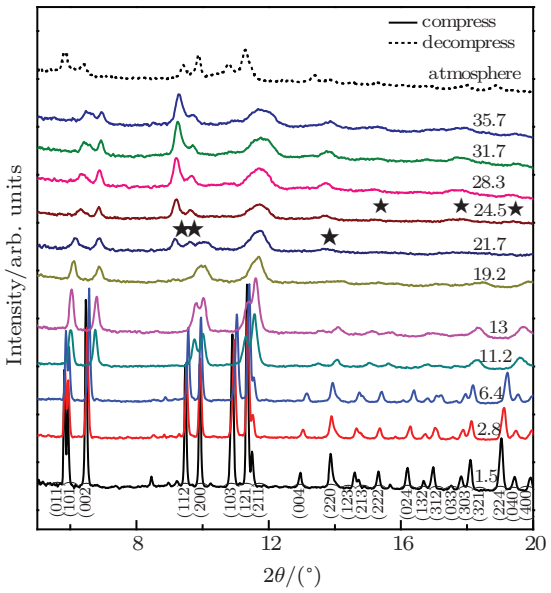



**Fig. 4.** (color online) XRD patterns collected at various pressues of $LiCuVO_4$ up to 35.7 GPa and then decompression to ambient pressure at room temperature. Pentagon symbols show the appearance of new Bragg peaks corresponding to a new phase.

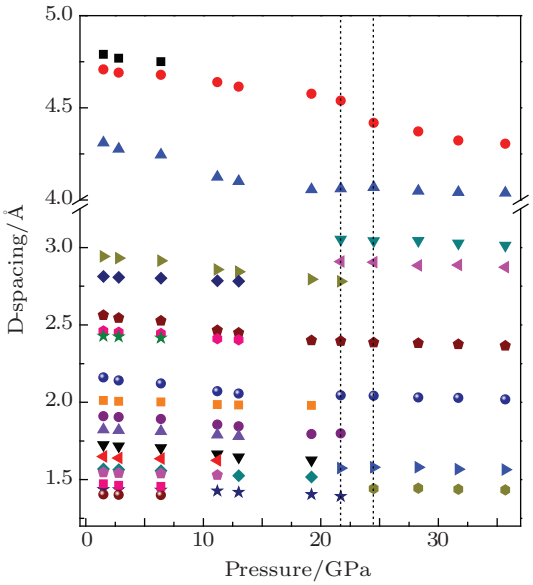



**Fig. 5.** (color online) D-spacing of $LiCuVO_4$ as a function of pressure at room temperature. The middle regions correspond to two phase coexistence.

The results of experimental and calculated comparison at 28.3 GPa are shown in Fig. 6(b), and it shows that the $LiCuVO_4$ high-pressure phase is a monoclinic structure. By the Pawley refinement results of the new phase data by each pressure, the pressure dependence of the volume of monoclinic high-pressure phases is described by a second-order Birch–Murnaghan equation of state:[26]

$$P = 3/2B_0[(V_0/V)^{7/3} - (V_0/V)^{5/3}] \times \{1 + 3/4(B_0' - 4) \times [(V_0/V)^{2/3} - 1]\}, \quad (1)$$

where $B_0$ is the bulk modulus, $B_0'$ is the pressure derivative, $V$ is the unit cell volume at pressure $P$, and $V_0$ is the zero-pressure volume.

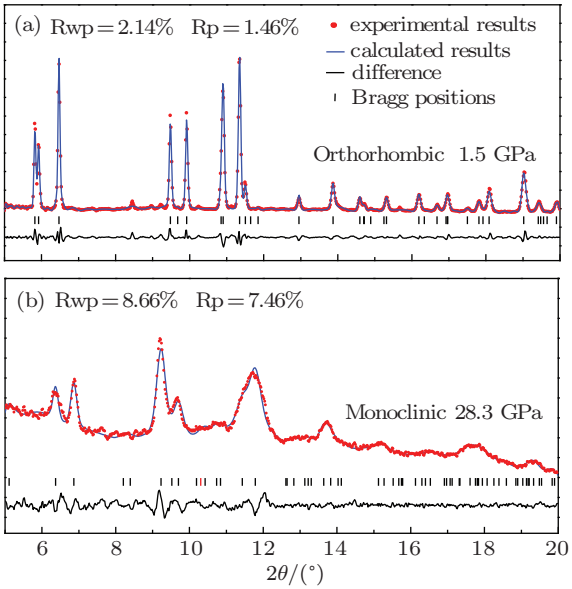



**Fig. 6.** (color online) Rietveld and Pawley refinement of the XRD patterns of $LiCuVO_4$ taken at 1.5 GPa and 28.3 GPa: (a) structural of the ambient orthorhombic structure with space group of *Imma*; (b) structural refinement of the high-pressure monoclinic phase.

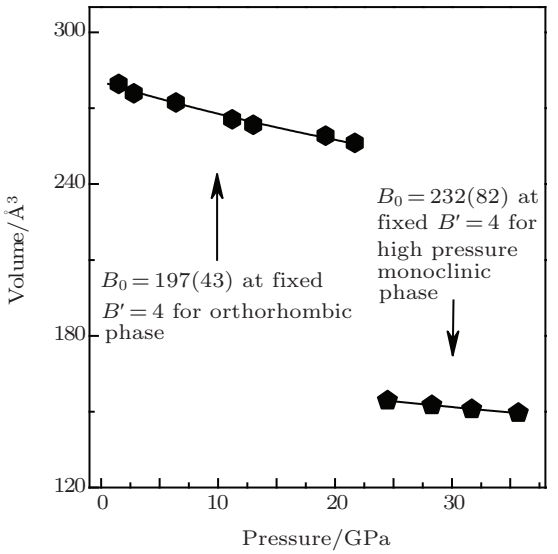



**Fig. 7.** Pressure dependence of cell volumes per formula unit of the orthorhombic phase and high pressure monoclinic phase structures of $LiCuVO_4$. The solid lines are the fitting results with the Birch–Murnaghan equation of state.

The bulk modulus $B_0$, obtained from a fitting of Eq. (1) to the data shown in Fig. 7. It shows that bulk modulus of the orthorhombic phase $B_0 = 197 \pm 9$ GPa, and $B_0 = 232 \pm 12$ GPa for high pressure monoclinic phase. Both pressure derivatives have been constrained to 4.0. The attempts to describe and predict spinel structural compression have led to the interpretation of the bulk modulus of the constituent cation-anion tetragonal and octahedral polyhedral. Recio *et al.*[27] and Finger *et al.*[28] suggested that all oxide spinels should have a similar value of the bulk modulus of about 200 GPa. In comparison, the bulk modulus of the proto type spinel $MgAl_2O_4$ is 196 GPa,[29] 197±5 GPa for $ZnMn_2O_4$[30] and 198±6 GPa for $CuMn_2O_4$,[31] because the observed bulk modulus indicates an average of polyhedral compressibilities between the tetrahedron and octahedron in the spinel structure. According to our work, the value of the bulk modulus 197(5) GPa provide a further evidence of this empirical suggestion. In the structure of oxide spinel, the oxygen ions form a nearly close packed sublattice, occupying most of the available space. The oxygen ions are relatively easy to deform, whereas the metal cations generally are more difficult to compress. In this way, the overall compressibility is determined mainly by the oxygen sublattice.[27] It is the essentially physical explanation of the conforming high pressure behavior of the oxide spinels.

## 4. Conclusion

An in-situ Raman spectroscopic and XRD study was carried out to explore the pressure-induced phase transformation of inverse spinel $LiCuVO_4$ to 40.3 GPa and 35.7 GPa, respectively. Results indicate that $LiCuVO_4$ undergoes a phase transformation from the orthorhombic phase to the monoclinic structure phase at pressures of 20–24.4 GPa, and this new high pressure phase remains stable to the pressure of 35.7 GPa. Upon release of pressure to ambient conditions, the high-pressure phase transforms back to the orthorhombic phase, which indicates that the transformation is reversible. The pressure dependence of the volume of monoclinic high-pressure phases is described by a second-order Birch–Murnaghan equation of state, which yields that the bulk modulus value of the orthorhombic phase and monoclinic phase were calculated to be $B_0 = 197(5)$ GPa and 232(8) GPa, respectively. The results show a good agreement with the empirical suggestion that the oxide spinels have almost the same bulk modulus around 200 GPa.

## Acknowledgment

The author is grateful to Wang Chun-Zhang and Bie Xiao-Fei for their help during the synthesis of the sample at the College of Physics, Jilin University. XRD measurements were carried out at the Cornell High Energy Synchrotron Source, Wilson Laboratory, Cornell University. CHESS is supported by NSF and NIH/NIGMS through a NSF award DMR-0936384.

## References

[1] Fey G T K and Huang D L 1999 *Electrochimica. Acta* **45** 295
[2] Fontijn W F J, van der Zaag P J, Feiner L F, Metselaar R and Devillers M A C 1999 *J. Appl. Phys.* **85** 5100

[3] Zerr AMiehe G, Serghiou G, Schwarz M, Kroke ERiedel R, Fuesz H, Kroll P and Boehler R 1999 *Nature* **400** 340
[4] Martinez S E, Garcia H M, Guzman J, Ramos B F, Santoyo S J, Martinez M R, Alvarez F O, Ramos C M I, Mendez D J J and Falcony C 2005 *Phys. Stat. Sol.* A **202** 102
[5] Liu Y, Zhou R, Li J, Zhang Y, Xiong R, Yin D, Tang W F and Shi J 2010 *Acta Phys. Sin.* **59** 5620 (in Chinese)
[6] Lafontaine M A, Leblanc M and Ferey G 1989 *Acta Crystallogr.* C **45** 1205
[7] Kanno R, Kawamoto Y, Takeda Y, Hasegawa M, Yamamoto O and Kinomura N 1992 *J. Solid State Chem.* **96** 397
[8] Schrettle F, Krohns S, Lunkenheimer P, Hemberger J, Büttgen N, Krug von Nidda H A, Prokofiev A V and Loidl A 2008 *Phys. Rev.* B **77** 144101
[9] Vasil'ev A, Ponomarenko L, Manaka H, Yamada I, Isobe M and Ueda Y 2001 *Phys. Rev.* B **64** 024419
[10] Kazakopoulos A and Kalogirou O 2008 *Solid State Ionics* **179** 936
[11] Moskvin A S and Drechsler S L 2008 *Europhys Lett.* **81** 57004
[12] Yukio Y, Kenji S, Taketo M, Masatoshi S and Kazuhisa K 2008 *J. Phys. Soc. Jpn.* **77** 023712
[13] Masatoshi S, Yukio Y, Yoshiaki K, Kenji S, Yutaka N, Yasuko T and Yuji K 2010 *Solid State Sci.* **12** 670
[14] Wang Z W, Lazor P, Saxena S K and Artioli G 2002 *J. Solid State Chem.* **165** 165
[15] Levy D, Pavese A, Sani A and Pischedda V 2001 *Phys. Chem. Miner.* **28** 612
[16] Errandonea D, Kumar R Manjón F, Ursaki V and Rusu E 2009 *Phys. Rev.* B **79** 024103
[17] Wang Z W, Downs R, Pischedda V, Shetty R, Saxena S, Zha C S, Zhao Y, Schiferl D and Waskowska A 2003 *Phys. Rev.* B **68** 094101
[18] Du F, Wang C Z, Li X, Li A and Chen G 2008 *Chem. J. Chin. Universities* **29** 1312
[19] Fey G T F and Huang D L 1999 *Electrochimica Acta* **45** 295
[20] MaoH K, Xu J and Bell P M 1986 *J. Geophys. Res.* **91** 4673
[21] Wang Z W, Chen O, Cao C Y, Finkelstein K, Smilgies D M, Lu X and Bassett W A 2010 *Rev. Sci. Instrum.* **81** 093902
[22] Jin E J, Yao L D, Wang F F and Shen X 2009 *Chin. J. H. P. Phys.* **23** 241 (in Chinese)
[23] Shirokov V B, Yuzyuk Y I, Torgashev V I and Prokhorov A S 2005 *Phys. Solid State* **47** 539
[24] Preudhomme J and Tarte P 1972 *Spectrochimica Acta Part A: Molecular and Biomolecular Spectroscopy* **28** 69
[25] Chen J Y, Zheng H F, Zhang H, Weng K N and Zeng Y S 2005 *Physics* **3** 221 (in Chinese)
[26] Birch F 1938 *J. Appl. Phys* **9** 279
[27] Recio J M, Franco R, Martín P A, Blanco M, Pueyo L and Pandey R 2001 *Phys. Rev.* B **63** 184101
[28] Larry W F, Robert M H and Anne M H 1986 *Phys. Chem. Miner.* **13** 215
[29] Kruger M B, Nguyen J H, Cadwell W and Jeanloz R 1997 *Phys. Rev.* B **56** 1
[30] Åsbrink S, Wa S A, Staun O J, Gerward L and Talik E 1999 *Phys. Rev.* B **60** 12651
[31] Waskowska A, Gerward L, Olsen J S, Steenstrupand S and Talik E 2001 *J. Phys. Condens. Matter* **13** 2549